Sensitivity analysis methodology for battery degradation models

Appiah, Williams Agyei; Busk, Jonas; Vegge, Tejs; Bhowmik, Arghya

Published in:
Electrochimica Acta

Link to article, DOI:
10.1016/j.electacta.2022.141430

Publication date:
2023

Document Version
Publisher's PDF, also known as Version of record

Electrochimica Acta 439 (2023) 141430

Contents lists available at ScienceDirect

Electrochimica Acta

journal homepage: www.journals.elsevier.com/electrochimica-acta

Sensitivity analysis methodology for battery degradation models

Williams Agyei Appiah[1], Jonas Busk[1], Tejs Vegge, Arghya Bhowmik *

Department of Energy Conversion and Storage, Technical University of Denmark, 301 Anker Engelunds vej, Kongens Lyngby, Copenhagen, 2800, Denmark

ARTICLE INFO

Keywords:
Solid electrolyte interphase
Pseudo-two-dimensional model
Lithium-ion battery
Sensitivity analysis
Gaussian process regression

ABSTRACT

Accurate degradation models are crucial to perform efficient battery design and management. The time and resources required to improve the output accuracy of the models depends critically on the ability to assess the sensitivity to the input factors governing the inherent dominant mechanism in the model. Here, we present a sensitivity analysis of a pseudo-two-dimensional battery model coupled with a capacity fade model based on solid-electrolyte interphase (SEI) formation and the corresponding irreversible charge loss for Li-ion batteries. The proposed method is based on training an inexpensive differentiable surrogate Gaussian process regression model on observed input–output pairs and analysing the surrogate model to learn about the global and local sensitivities of the original system. With this method, the relevant global sensitive parameters can be identified, and an in-depth analysis of electrochemical phenomena such as the correlation between the thickness of the SEI and the irreversible charge loss can be explored. The proposed method will provide key insight into how sensitivity analysis of the physics-based degradation model must be conducted for effective integration into battery management systems.

1. Introduction

Li-ion batteries (LIBs) dominate the secondary electrochemical energy storage market for both mobile (electric vehicles) and stationary (grid storage) applications. State of the art in battery research focuses on deducing parameters that are key to battery performance and developing design principles accordingly [1–3]. The LIB performance, durability and reliability depend on broad range of multi-scale phenomena [4]. Design of better LIBs [5] thus require multi-scale modelling methods [6,7] for optimal utilisation, degradation control and safety. Multi-scale modelling relies on parameter passing between scales [7]. Within the scale-bridging approach, for each scale-specific physical model, identifying parameters to which the model is most sensitive can make such an approach robust to input parameter noise and make it uncertainty aware. On the other hand, at system level, battery management systems (BMSs) are crucial for operational time optimisation. To ensure accurate predictions and estimation of relevant metrics, such as battery state of charge (SOC) and state of health (SOH), coupled physics-based and degradation models need to be integrated into BMSs. However, physics-based models contain several input parameters obtained from experiments and other simulations conducted at a lower scale, with different degrees of sensitivity to the main output parameters in the degradation model resulting in an uncertainty in the overall predictions. These uncertainties can be reduced by performing sensitivity analysis (SA) to identify relevant input parameters and the main sources of uncertainty.

SA in general studies how variation in the inputs of a given system affects its outputs and can be done at different levels of complexity and sampling cost ranging from inexpensive screening for irrelevant inputs to detailed exploration of the effect of inputs along their entire range of variation [8]. Local SA methods focus on how a single set of input parameters affects the output, for example the partial derivative of the model at a specific point can be estimated by slightly varying the input and observing the output (aka. the one-at-a-time method), while global SA methods aim to understand the behaviour of the overall system, or at least within a some specified range of values for each input parameter. A global SA can be achieved by fitting a surrogate model on observed pairs of inputs and outputs and then analysing the surrogate model in place of the original system, which is especially useful when the surrogate model is cheaper to evaluate and easier to analyse than the original system. An accurate surrogate model can subsequently be used for detailed local SA in specific regions of input space and to suggest new input parameters to evaluate.

In this work, we present a SA of a pseudo-two-dimensional (P2D) battery model coupled with a capacity fade model based on the formation of solid-electrolyte interphase (SEI) and the corresponding irreversible charge loss (ICL) for LIBs. The aim is to apply SA using a

* Corresponding author.
E-mail address: arbh@dtu.dk (A. Bhowmik).
[1] Equal contribution.

https://doi.org/10.1016/j.electacta.2022.141430
Received 11 August 2022; Received in revised form 18 October 2022; Accepted 22 October 2022
Available online 2 November 2022

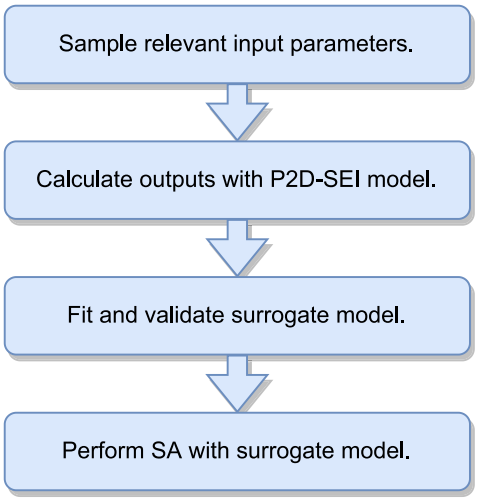

Fig. 1. Overview of the data generation and sensitivity analysis procedure.

surrogate model to identify the globally most sensitive input parameters causing SEI formation and related ICL and to explore local sensitivities and interactions in critical parts of the input space (see Fig. 1). The results of the SA can guide further efforts to obtain high-fidelity estimates of important input parameters to improve errors and ensure accurate predictions.

Analysis of battery models is an area of interest in recent research. Schmidt et al. [9] used a coupled Fisher-information matrix approach and local SA method to identify the dependence of each selected input parameter on the output parameter of a physics-based single particle model (SPM). The local SA of the input parameters on the terminal voltage of an equivalent circuit model (ECM) for LIBs was conducted by Rahimi-Eichi et al. [10] to determine the importance of updating each battery parameter in a state of charge (SOC) estimation structure. However, because some of the parameters in SPM and ECM are functions of the SOC, local SA is not suitable for evaluating their robustness since this does not reflect how the system behaves in other regions of input space where seemingly unimportant inputs may have a large effect and vice versa. Global SA methods are suitable for ECM especially for the non-linear P2D models because global SA repeatedly analyse local sensitivity multiple times with randomly sampled linearisation points [11]. Zhang et al. [11] carried out a SA on the terminal voltage and temperature of a cylindrical Li-ion battery based on a thermally coupled multi-physics based model via step-wise experiments where thirty input parameters were grouped according to their maximum sensitivity. Similarly, Song et al. [12] conducted a SA of parameters to the rate of heat generation in LIBs based on a reduced-order electrochemical–thermal model where they observed that parameters related to the positive electrode are more sensitive than those related to the negative electrode based on the selected range of input parameters. None of these works considered the sensitivity of the various input parameters of the electrochemical model on the capacity fading parameters such as the thickness of the SEI. Even though the capacity loss due to the formation of the SEI is considered as the main factor responsible for capacity fading in LIBs. Zhao and Howey [13] investigated the global sensitivity of ECM model input parameters on the output voltage of a battery using Morris screening methods [14] where they found out that, the uncertainties of some of the parameters do not generate significant uncertainty in the out voltage and therefore could be taken as constants. However, they could not investigate the interactions between the parameters due to the limitation of the approach used. Lin et al. [15] performed a global SA of the cell discharge capacity and temperature based on a 3D multi-physics model using the concept of a polynomial chaos expansion (PCE) where they observed that, the discharge capacity and the thermal behaviour of the cell are more sensitive to the electrode parameters and their pore structure. However, PCE suffers from the curse of dimensionality [16], that is the model evaluations needed to develop the PCE model increases exponentially with the number of model parameters.

Gaussian process (GP) regression [17] is a popular choice of surrogate model in SA because it is highly flexible, provides uncertainty estimates and can be applied even with small datasets while approximate, sparse implementations enable analysis of large datasets [18,19]. Automatic relevance determination (ARD) of GPs with isotropic kernels has been a widely used method to evaluate feature importance, but recent work has shown how ARD overestimates the importance of features with nonlinear effects on the output, while SA based on derivatives of the GP output with regards to the inputs has been shown to be robust to a mix of linear, nonlinear and noise features [20]. Measuring sensitivity by derivatives makes intuitive sense since if changing an input parameter is expected to significantly change the output, it is important to consider that input parameter carefully. SA methods based on analysing derivatives of GP regression models have previously been applied for analysing neuroimages [21] and global ocean chlorophyll prediction [22] showing promising results.

In this paper we present a P2D-SEI model for the formation of the SEI and prediction of the related ICL and apply global and local SA using a surrogate GP regression model to identify interesting regions of input space. The main contributions are:

- A P2D-SEI capacity fade model that simulates SEI formation and related ICL together.
- Application of a scalable SA approach based on analysing the derivatives of a surrogate GP regression model enabling global and local analysis of sensitive input parameters.
- Software demonstrating an interactive, explorative SA of a surrogate GP regression models for SEI thickness and ICL made available online [23].

The rest of the paper is structured as follows. Section 2 presents the computational methods used in the analysis including the P2D battery degradation model and the SA method based on GP regression. The experiment and results are presented and discussed in Section 3, and we conclude with closing remarks in Section 4.

2. Methods

2.1. Modelling SEI formation

The model for the formation of the SEI used in this study is based on the reduction of the solvent near the surface of the negative electrode during charging. The electrolyte considered in the model is a mixture of ethyl carbonate/ethyl methyl carbonate (EC/EMC) with $LiPF_6$ salt. Hence, we assumed that the primary product forming the SEI layer is Li_2CO_3 [24] and it is formed according to the reaction:

$$S + 2Li^+ + 2e^- \xrightarrow{k} P, \tag{1}$$

where S is the solvent species and P is the product of the reaction between the solvent and the Li ions. The growth of the SEI layer is assumed to be in one-dimension as illustrated in Fig. 2 and the film growth is assumed to be controlled by the kinetics of the reaction occurring at the interphase.

The rate of the electrochemical reaction at the negative electrode is described as the sum of the rate of reaction for Li intercalation and the rate of reaction for the formation of the SEI which is expressed in terms of their current densities as:

$$J = J_{\text{int}} + J_s. \tag{2}$$

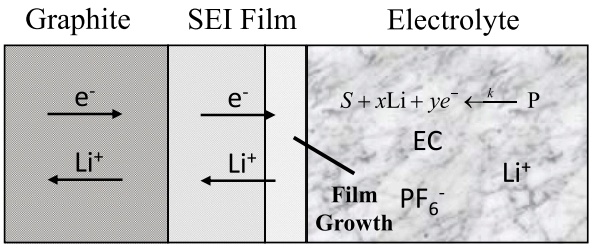

Fig. 2. Schematic diagram of SEI formation.

The current density due to the intercalation of Li ions across the electrode/electrolyte interface, J_{int} is described by the Butler Volmer (BV) equation and is given by:

$$J_{\text{int}} = i_0 a_p \left(\exp\left[\alpha_a \frac{F}{RT}(\eta)\right] - \exp\left[-\alpha_c \frac{F}{RT}(\eta)\right] \right), \tag{3}$$

where i_0 is the concentration dependent equilibrium exchange current density at the interface and is given by:

$$i_0 = i_{0,\text{ref}} \left(\frac{c_s}{c_{s,\text{ref}}}\right)^{\alpha_c} \left(\frac{c_{s,\max} - c_s}{c_{s,\max} - c_{s,\text{ref}}}\right) \left(\frac{c_e}{c_{e,\text{ref}}}\right), \tag{4}$$

where c_s, $c_{s,\max}$, and c_e are the surface, maximum and electrolyte concentration respectively. The overpotential for the intercalation reaction is given by:

$$\eta = \phi_s - \phi_l - U_{\text{ref}} - \frac{J}{a_p} R_{\text{film}}, \tag{5}$$

where ϕ_s, ϕ_l, and U_{ref} are the potential in the solid and liquid phase, respectively. R_{film} is the resistance due to the formation of the SEI layer, and U_{ref} is the equilibrium potential of the negative electrode expressed as a function of the state of charge (SOC), θ.

The rate of the solvent reduction reaction in Eq. (1) was also described by the BV equation and is given by:

$$J_s = i_{os} a_p \left(\left(\frac{c_p}{c_{p,\text{ref}}}\right) \exp\left[\alpha_a \frac{F}{RT}(\eta_s)\right] - \left(\frac{c_s}{c_{s,\text{ref}}}\right) \left(\frac{c_{\text{Li}^+}}{c_{\text{Li}^+,\text{ref}}}\right)^2 \exp\left[-\alpha_c \frac{F}{RT}(\eta_s)\right] \right). \tag{6}$$

The side reduction reaction is assumed to be irreversible and hence the BV equation is reduced to cathodic Tafel approximation, and the rate of the reaction is given by:

$$J_s = -i_{os} a_p \left(\frac{c_s}{c_{s,\text{ref}}}\right) \left(\frac{c_{\text{Li}^+}}{c_{\text{Li}^+,\text{ref}}}\right)^2 \exp\left[-\alpha_c \frac{F}{RT}(\eta_s)\right]. \tag{7}$$

At low current rates, the variation in the concentration of Li ions in the solution does not vary much. In addition, the concentration of Li ions and solvent is in excess and hence not a limiting factor for the side reaction. In view of the above assumptions, the cathodic Tafel rate kinetics is modified to eliminate the concentration dependencies and the final rate expression is expressed as:

$$J_s = -i_{os} a_p \exp\left[-\alpha_c \frac{F}{RT}(\eta_s)\right]. \tag{8}$$

The overpotential for the side reaction, η_s is expressed as:

$$\eta_s = \phi_s - \phi_l - U_{\text{ref},s} - \frac{J}{a_p} R_{\text{film}}. \tag{9}$$

The film resistance, R_{film} due to the formation of the SEI film is expressed as:

$$R_{\text{film}} = \frac{\delta_{\text{film}}}{\sigma_p}, \tag{10}$$

where σ_p is the conductivity of the SEI products and δ_{film} is the thickness of the SEI film and is expressed as:

$$\frac{\partial \delta_{\text{film}}}{\partial t} = -\frac{J_s M_p}{a_p \rho_p F}, \tag{11}$$

where M_p and ρ_p is the molecular weight and density of the product of the side reaction, Li_2CO_3. The developed SEI model was incorporated into the P2D model. An overview of the governing equations, boundary, and initial conditions of the P2D model is presented in Table 1. The model equations were solved in COMSOL Multiphysics 5.6.

2.2. Gaussian process regression

In the SA we consider a surrogate GP regression model trained on observed inputs and outputs of the P2D-SEI model. Generally in a supervised regression setting, we observe input–output pairs $\{(\mathbf{x}_n, y_n)\}_{n=1}^N$ with input vectors $\mathbf{x}_n \in \mathbb{R}^D$ and real-valued output labels $y_n \in \mathbb{R}$. We assume that $y_n = f(\mathbf{x}_n) + \epsilon$ for some unknown function f with added Gaussian noise $\epsilon \sim \mathcal{N}(0, \sigma_y^2)$. A GP regression model defines a prior distribution over such functions and is completely specified by its mean function m and covariance function (aka. kernel) k [17]:

$$f(\mathbf{x}) \sim GP\big(m(\mathbf{x}), k(\mathbf{x}, \mathbf{x}')\big). \tag{12}$$

The mean function represents an initial guess at the regression function and the covariance function specifies the covariance between any two points. Here we use a zero mean function $m(\mathbf{x}) = 0$ and the widely used (scaled) squared exponential (SE) covariance function (aka. the RBF kernel) for noisy observations:

$$k_{\text{SE}}(\mathbf{x}_p, \mathbf{x}_q) = \sigma_f^2 \exp\Big(-\frac{1}{2}(\mathbf{x}_p - \mathbf{x}_q)^T \text{diag}(\ell)^{-2}(\mathbf{x}_p - \mathbf{x}_q)\Big) + \sigma_y^2 \delta_{pq}, \tag{13}$$

where the hyper-parameters σ_f^2 controls the magnitude, $\ell \in \mathbb{R}^D$ represents the length-scales and controls the smoothness along each input dimension, σ_y^2 is the noise variance and δ_{pq} is defined as 1 if $p = q$ and 0 otherwise.

The GP posterior mean $\mu_{\text{GP}}(\mathbf{x}_n)$ and variance $\sigma_{\text{GP}}^2(\mathbf{x}_n)$ can be inferred by conditioning on observed data and the hyper-parameters can be optimised with gradient-based methods [17]. For GP regression on small to medium sized datasets, the posterior mean and variance can be computed in closed form. However, for large datasets this is not feasible due to the expensive matrix operations involved. Therefore, in practice we use approximate sparse GP regression to be able to scale the approach to larger datasets [18,19].

2.3. Sensitivity analysis with GP regression

In the SA of the surrogate model we want to measure the expected change in the predicted output as a function of the input parameters. In the context of the GP regression model, we are primarily interested in measuring the sensitivity of the mean function μ_{GP} and secondly in the variance function σ_{GP}. The (local) sensitivity of function g with regards to input parameter d at a single query point $\tilde{\mathbf{x}}_n$ can be computed as the squared derivative of g with regards to input parameter d [21,22]:

$$s_{n,d}^2(g) = \left(\frac{\partial g(\tilde{\mathbf{x}}_n)}{\partial \tilde{x}_{n,d}}\right)^2. \tag{14}$$

Notice that the query point does not have to be in the dataset but can be anywhere in input space. The partial derivative in the expression above can be computed analytically for GP regression with some covariance functions, such as the SE covariance function, or with automatic differentiation [27] allowing for more flexibility in defining the model.

To summarise the sensitivity across the input space, the global sensitivity $s_{*,d}^2(g)$ of function g with regards to input parameter d can be computed empirically by averaging over a set of input samples [21,22]:

$$s_{*,d}^2(g) = \frac{1}{N} \sum_{n=1}^{N} s_{n,d}^2(g). \tag{15}$$

To allow direct comparison of sensitivities of input parameters with different scales, the input data should be normalised. For visual presentation of sensitivities of different input parameters, for example

Table 1
An overview of the P2D model equations, boundary and initial conditions [25,26].

Cell compartment	Balance	Governing equations	Boundary or initial condition
Positive electrode	Material, solid phase	$\frac{\partial c_{s,p}}{\partial t} = D_{s,p}\frac{1}{r^2}\frac{\partial}{\partial r}\left(r^2\frac{\partial c_{s,p}}{\partial r}\right)$	$c_{s,p}\big\|_{t=0} = c_{p,\mathrm{ini}}$, $-D_{s,p}\frac{\partial c_{s,p}}{\partial r}\big\|_{r=0} = 0$, $-D_{s,p}\frac{\partial c_{s,p}}{\partial r}\big\|_{r=R_p} = j$
	Charge, solid phase	$\sigma_{s,p}^{\mathrm{eff}}\frac{\partial \phi_{1,p}}{\partial x^2} = a_{s,p}Fj$	$\sigma_{1,p}\big\|_{x=L_p} = 0$, $-\sigma_{\mathrm{eff},n}\frac{\partial \phi_{1,p}}{\partial x}\big\|_{x=L_s} = 0$
	Material, liquid phase	$\epsilon_{e,p}\frac{\partial c_{e,p}}{\partial t} = \frac{\partial}{\partial x}\left(D_{\mathrm{eff},p}\frac{\partial c_{e,p}}{\partial x}\right) + \left(1-t_+^0\right)a_{s,p}j$	$c_e\big\|_{t=0} = \mathbf{c_{e,0}}$, $-D_{\mathrm{eff},p}\frac{\partial \mathbf{c_{e,p}}}{\partial x}\big\|_{x=L_p} = 0$, $-D_{\mathrm{eff},p}\frac{\partial \mathbf{c_{e,p}}}{\partial x}\big\|_{x=L_s} = -D_{\mathrm{eff},s}\frac{\partial \mathbf{c_{e,p}}}{\partial x}\big\|_{x=(L_p+L_s)}$
	Charge, liquid phase	$-\frac{\partial}{\partial x}\left(\kappa_{\mathrm{eff},p}\frac{\partial \phi_{2,p}}{\partial x}\right) + \frac{2RT(1-t_+^0)}{F}\frac{\partial}{\partial x}\left(\kappa_{\mathrm{eff},p}\frac{\partial \ln c}{\partial x}\right) = a_{s,p}F$	$-\kappa_{\mathrm{eff},p}\frac{\partial \phi_{2,p}}{\partial x}\big\|_{x=L_p} = 0$, $-\kappa_{\mathrm{eff},p}\frac{\partial \phi_{2,p}}{\partial x}\big\|_{x=L_p} = -\kappa_{\mathrm{eff},s}\frac{\partial \phi_{2,s}}{\partial x}\big\|_{x=L_p}$
Separator	Material, liquid phase	$\epsilon\frac{\partial c_e}{\partial t} = \frac{\partial}{\partial x}\left(D_{\mathrm{eff},s}\frac{\partial c_e}{\partial x}\right)$	$c_e\big\|_{t=0} = c_{e,0}$, $-D_{\mathrm{eff},n}\frac{\partial c_e}{\partial x}\big\|_{x=0} = -D_{\mathrm{eff},s}\frac{\partial c_e}{\partial x}\big\|_{x=L_p}$, $-D_{\mathrm{eff},s}\frac{\partial c_e}{\partial x}\big\|_{x=(L_s)} = -D_{\mathrm{eff},p}\frac{\partial c_e}{\partial x}\big\|_{x=(L_p+L_s)}$
	Charge, liquid phase	$-\kappa_{\mathrm{eff},s}\frac{\partial \phi_{2,s}}{\partial x} + \frac{2Rt(1-t_+^0)}{F}\kappa_{\mathrm{eff},s}\frac{\partial \ln c_e}{\partial x} = 0$	$-\kappa_{\mathrm{eff},s}\frac{\partial \phi_{2,s}}{\partial x}\big\|_{x=(L_s+L_p)} = -\kappa_{\mathrm{eff},p}\frac{\partial \phi_{2,p}}{\partial x}\big\|_{x=(L_s+L_p)}$, $-\kappa_{\mathrm{eff},p}\frac{\partial \phi_{2,p}}{\partial x}\big\|_{x=L_s} = -\kappa_{\mathrm{eff},s}\frac{\partial \phi_{2,s}}{\partial x}\big\|_{x=(L_s+L_p)}$

as a bar chart, we have found it useful to consider the square root of the sensitivities $s_{*,d}(g)$ (the root mean squared derivative) to not underestimate the importance of input parameters with relatively low sensitivity and to be able to distinguish between small sensitivities and sensitivities that are practically zero.

3. Results and discussion

3.1. P2D-SEI model predictions

During the discharge of the Li ion half-cell, a negative constant current is applied to oxidise Li ions at the Li metal and intercalate into the graphite. This results in a gradual decrease in the potential of the cell until when almost all the available intercalating sites have been occupied (at a state of charge of 1). At this point the cell reaches the minimum cut off potential of 0 V and then a positive constant current is applied to de-intercalate the Li ions from the graphite and reduced at the Li metal. The de-intercalation or reduction process proceeds until a cut-off potential of 1.5 V. At this potential, all the Li ions are assumed to be deintercalated and reduced resulting in an equal intercalation and de-intercalation time. However, the intercalation time is longer than that of the de-intercalation indicating that not all the intercalated Li ions were extracted. The trapped Li ions are consumed to form the SEI according to Eq. (1) and the rate of consumption is described by Eq. (8). The voltage profile and the applied constant current describing the (de-)intercalation mechanism corresponds to the following redox reaction:

$$\mathrm{C_6} + x\mathrm{Li^+} + xe^- \underset{\text{de-intercalation}}{\overset{\text{intercalation}}{\rightleftharpoons}} \mathrm{Li}_x\mathrm{C_6}\,. \tag{16}$$

Fig. 3a shows the simulated voltage profiles during the (de-) intercalation. The simulation was performed with the parameters presented in Table 2. The formation of the SEI product results in an increase in the thickness of the SEI layer on the graphite as presented in Fig. 3b. As recently discussed [6], the SEI is complex and modelling it requires the consideration of the effect of the various compositions on the electrochemical performance of LIBs. However to reduce the complexity and facilitate fast model predictions, the primary product of the SEI layer was assumed to be Li_2CO_3 [24] and only grows during the intercalation process, thus its thickness was constant during the de-intercalation process. Owing to the formation of the SEI, the charge capacity (capacity obtained during the intercalation process) was higher than that of the discharge capacity (capacity obtained during the de-intercalation process). The difference between the charge and discharge capacity is the ICL and is mainly attributed to the formation of the SEI layer. The SEI thickness and ICL obtained from the simulation are comparable what has been obtained experimentally [28,29].

There are several factors which affect the formation of the SEI at the surface of the graphite electrode during charging owing to the competition between the numerous reduction processes. The rates of the electrochemical reaction for the (de-)lithiation process and the SEI formation is greatly influenced by both the intrinsic properties of the reactants such as the exchange current densities, reductive potential and reduction activation energy, and the operating condition parameters such as the temperature, concentration of electrolyte and reduction current rate [30]. To understand the degree of the impact of these design parameters on the electrochemical performance of the cell and the SEI formation, we conducted a detailed SA of all the input parameters on the SEI thickness and ICL using a surrogate GP regression model.

3.2. High throughput simulation

The SA method proposed in Section 2.3 was applied in a detailed analysis of the P2D-SEI model introduced in Section 2.1. An overview of the method is presented in Fig. 1. We considered a total of 15 input parameters (see Table 2) that were hypothesised to contribute significantly to the output parameters of interest: (i) *SEI thickness (m)* representing the thickness of the SEI layer, and (ii) *Irreversible charge loss (%)* representing the ICL due to SEI formation. The input parameters can be categorised into parameters based on the P2D model for the positive electrode; applied current density, particle radius, porosity, diffusion coefficient of Li ion in the electrolyte, exchange current density, minimum cut-off potential, initial concentration of Li ions in the electrolyte, transference number, maximum concentration of Li and electronic conductivity, that of the negative electrode; the exchange current density, and those of the SEI-based model; SEI film conductivity, equilibrium potential for the SEI and the exchange current density of the SEI. Based of the data obtained from literature, reasonable boundaries of each input parameter were identified as well as a nominal input value (see Table 2). The equilibrium potential for the negative electrode was not considered because it is expressed as a function of the state of charge (SOC).

A dataset of input–output pairs was generated by sampling 30,000 sets of input parameters uniformly at random within the input ranges defined in Table 2. The corresponding output values were computed by querying the P2D-SEI model resulting in a labelled dataset of 23,074 examples, since not all input configurations converged due to the non-physicality of some of the generated input parameters. The labelled dataset was then split into a training dataset of $N_{\mathrm{train}} = 20{,}000$ examples and a validation dataset of the remaining $N_{\mathrm{valid}} = 3074$ examples reserved for model evaluation. Since both of the target outputs consist of non-negative values by definition, we transform them by the base 10 logarithm (log) to put them on an unbounded scale and thus simplify the modelling and avoid non-physical, negative predictions. To enable direct comparison of the results for each input parameter and to further simplify modelling, all inputs were normalised to values between zero and one using the minimum and maximum values given in Table 2 and the outputs were normalised to zero mean and unit variance using statistics derived from the training data before training the surrogate model.

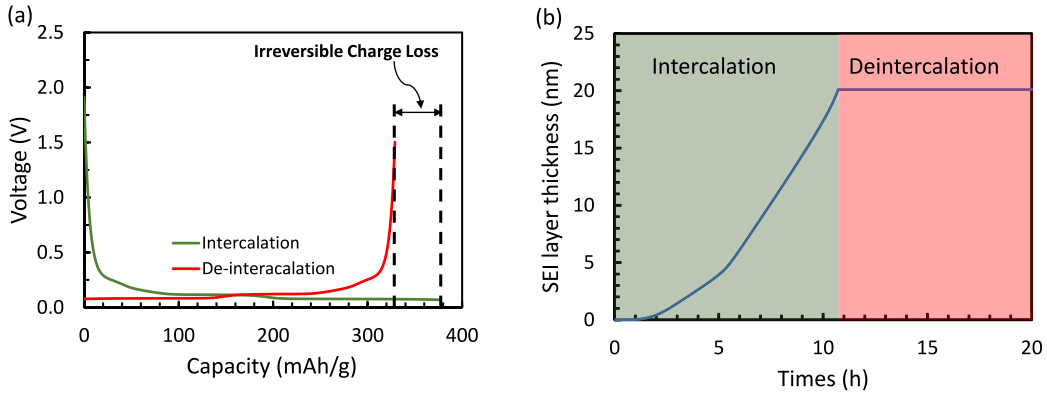

Fig. 3. (a) Simulated voltage profile for interaction and de-intercalation process of Li ion half cell with graphite positive electrode and Li metal negative electrode, and (b) related SEI layer thickness.

Table 2
List of P2D-SEI model input parameters and their minimum, maximum and nominal values considered in the sensitivity analysis. The values are determined from previous related works.

d	Parameter	Description	Minimum	Maximum	Nominal	Unit	References
1	i_app	Applied current	0.13	6.5	1.3	A	[31]
2	rp_pos	Particle radius	1×10^{-6}	1.1×10^{-5}	5.5×10^{-6}	μm	[12]
3	Eeq_side	Equilibrium potential (SEI)	0	0.4	0.4	V	[32–35]
4	kappa_film	SEI film conductivity	1×10^{-6}	2.4×10^{-4}	2.4×10^{-4}	S/m	[32–35]
5	epsl_pos	Porosity of positive electrode	0.23	0.4	0.3	–	[12]
6	Dl_elect	Electrolyte diffusion coefficient	1.5×10^{-10}	7.5×10^{-10}	3.75×10^{-10}	m^2/s	[12]
7	Ds_pos	Diffusion coefficient of Li in positive electrode	1×10^{-14}	1×10^{-13}	3.6×10^{-14}	m^2/s	[12]
8	i0ref_pos	Exchange current density of positive electrode	0.36	3.6	0.96	A/m^2	[12]
9	E_min	Minimum cut-off voltage	0.0	0.1	0.05	V	[36]
10	i0_SEI	SEI exchange current density	8×10^{-8}	1.5×10^{-6}	4.5×10^{-7}	A/m^2	[33,35,37]
11	csmax_pos	Maximum Li concentration	2.9×10^4	3.3×10^4	3.15×10^4	mol/m^3	[12]
12	cl_0	Initial electrolyte concentration	1000	1200	1150	mol/m^3	[38]
13	t_plus	Transference number	0.25	0.43	0.363	–	[39]
14	i0ref_metal	Li metal exchange current density	50	100	100	A/m^2	
15	sigma_pos	Electronic conductivity	50	100	100	S/m	[12]

3.3. Data exploration

Fig. 4 shows a scatter plot of the two outputs of interest: the SEI thickness and the ICL. It is apparent that an increase in the SEI thickness entails an increase in the ICL, which fits our hypothesis that the consumption of Li ions to form the SEI leads to ICL. Interestingly, it can be observed from Fig. 4 that there are also some high values of ICL at low values of SEI thickness, indicating that other input parameters not related to SEI formation can also cause an increase in the ICL. This is because a reduction in some of the input parameters, such as the porosity of the electrode, the radius of the active material, diffusivity of Li ions and maximum concentration of Li ions, also leads to capacity fade due to other mechanisms such as loss of active materials in the electrode and loss of active Li ions [40–42]. Such capacity fade degradation mechanisms, even though not considered in the P2D-SEI model, can still be observed during the data exploration because of the variation in the input parameters of the P2D model which are considered as descriptors for these mechanisms. However, the main focus of this work is to analyse the impact of these parameters on the SEI thickness and the corresponding ICL. A full scatter matrix of all the input and output samples is included in the supplementary material.

3.4. Evaluation of surrogate model

As the surrogate model we applied a sparse GP regression model from the Pyro probabilistic programming library [43] for Python (Python 3.9.6, PyTorch 1.9.0, Pyro 1.8.0). As a simpler baseline model we additionally applied a Bayesian linear regression model with Gaussian priors, likewise implemented using Pyro. Both models were trained with stochastic variational inference (SVI) using the ADAM optimiser with a learning rate of 0.01.

To ensure the validity of the SA, we evaluated the predictive performance of the surrogate GP regression model on the two targets of interest and compared it to a Bayesian linear regression model baseline. Both models were evaluated by fitting the models with the training dataset and computing the coefficient of determination R^2 on the validation dataset, which measures the proportion of variation in the output explained by the model as a score between 0 and 1 where 1 indicates a perfect fit.

The Bayesian linear regression baseline achieved a good fit on the log SEI thickness with an $R^2 = 0.96$ indicating a strong linear relationship between the input parameters and this output. However, the Bayesian linear regression model achieved a considerably lower $R^2 = 0.70$ on the log ICL, indicating a poor fit of the data and consequently the Bayesian linear regression model is not an appropriate surrogate model for this task. The GP regression model achieved $R^2 = 0.99$ on the log SEI thickness and an $R^2 = 0.98$ on the log ICL, indicating a good fit of the data in both cases. The distribution of the GP regression model predictions on the validation dataset is presented in Fig. 5 and a corresponding figure showing the Bayesian linear regression predictions are included in the supplementary material. The high predictive performance of the GP regression model indicates that it is able to capture the dynamics of the original system, which enables us to consider it as an accurate surrogate model in place of the original P2D-SEI model in the SA presented in the next sections.

3.5. Global sensitivity analysis

To quantify and compare the sensitivity of each input parameter overall, the global sensitivities with respect to log SEI thickness and

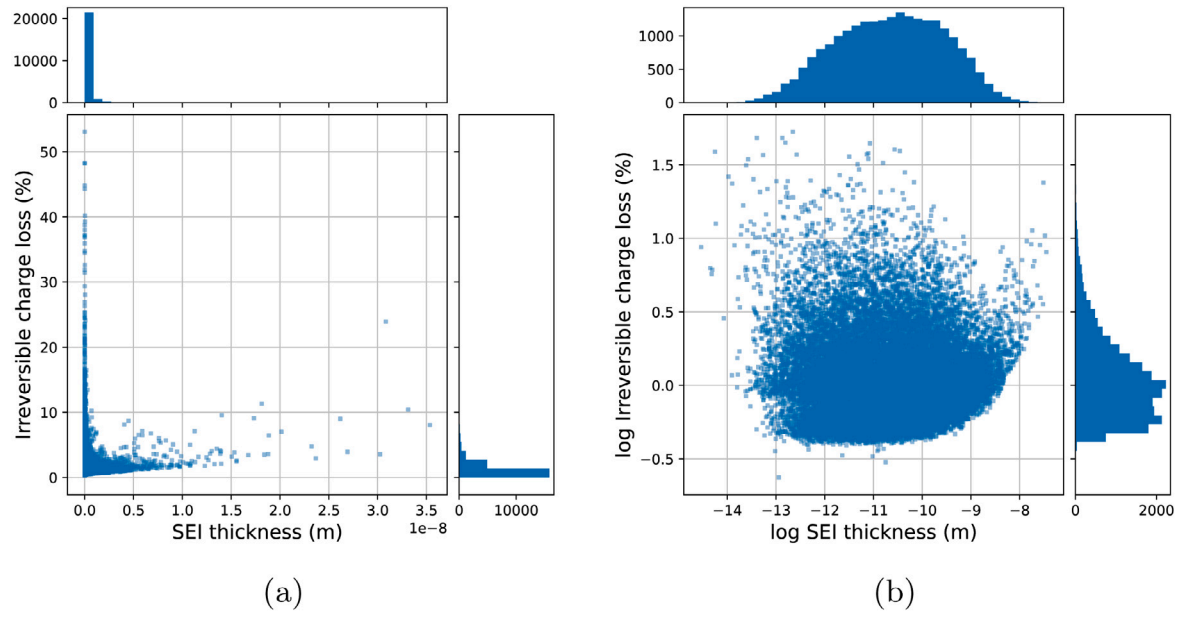

Fig. 4. Relationship between the two P2D-SEI model outputs of interest, the SEI thickness and the ICL, computed with different randomly sampled sets of input parameters, presented on (a) the original scale, and (b) log scale. An increase in the SEI thickness correlate with an increase in the ICL, however, there are also high values of ICL at low values of SEI thickness.

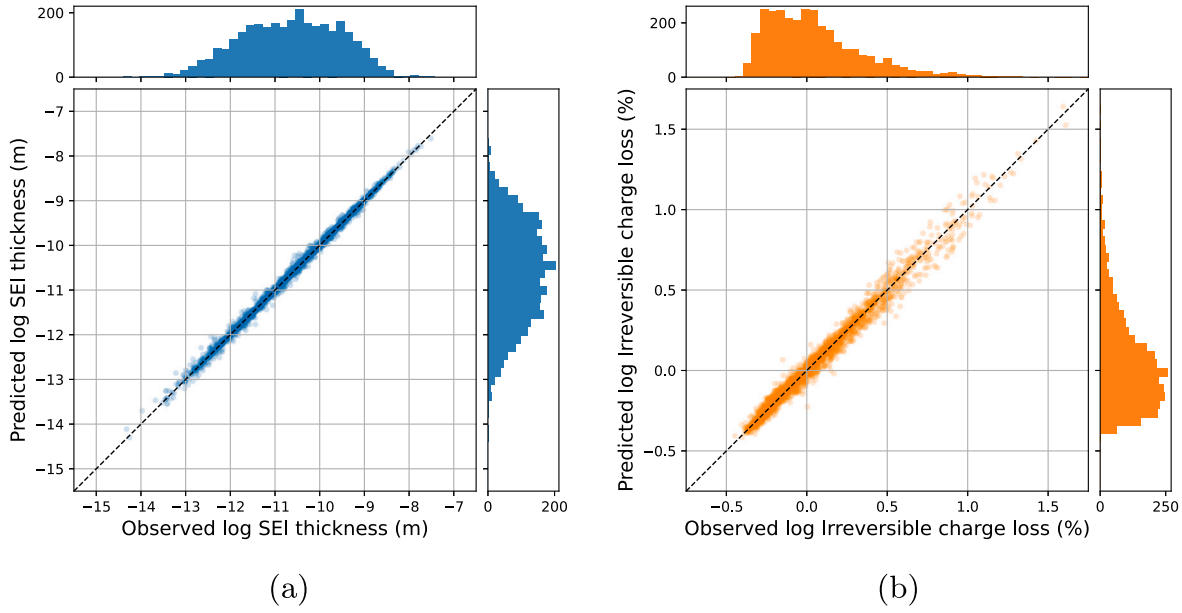

Fig. 5. Scatter plots of (a) observed and predicted log SEI thickness, and (b) log ICL on the validation dataset using the GP regression surrogate model. In both cases the observed and predicted values are highly correlated, with $R^2 = 0.99$ and $R^2 = 0.98$, respectively.

log ICL were computed using Eq. (15) and the surrogate GP regression model on the validation dataset (Fig. 6). Based on these results, the applied current density, the equilibrium potential, the minimum cut-off potential and the exchange current density were identified as the most sensitive input parameters to the SEI thickness. The remaining 11 parameters showed little or negligible sensitivity to the log SEI thickness. Out of these four parameters, two are directly related to the rate of the formation of the SEI (SEI model-based input parameters); the equilibrium potential and the exchange current density of SEI. Based on the Tafel equation, Eq. (8), used to describe the rate of the SEI formation, a variation in the exchange current density and the equilibrium potential of the SEI causes a linear and exponential variation in the SEI thickness respectively and hence the different degree of sensitivity. The increase in the SEI thickness due to changes in the exchange current density can be related to overcharge of graphite electrodes for cells with excess cyclable Li-ions owing to either higher than desired initial mass ratio or lower than expected Li-ions loss during the formation period [44]. While the other two are related to the operating conditions of the cell: the applied current density and the minimum cut-off potential. An increase in the applied current density exponentially accelerate the increase in the thickness of the SEI owing to an increase in the rate of SEI formation while the minimum cut-off potential dictates the amount of Li-ions inserted into the graphite at a given current density and thus the quantity of Li-ions consumed to form the SEI.

The global SA conducted on the log ICL identified six input parameters with high average sensitivity and three additional input parameters showing significant effects. The six parameters were the applied current

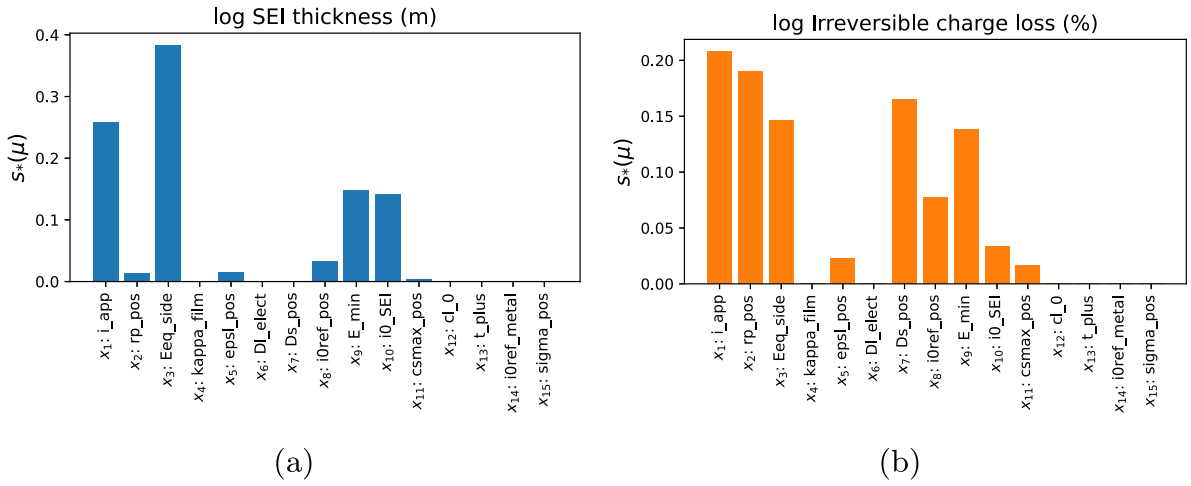

Fig. 6. Normalised global sensitivities computed on the validation dataset for (a) the log SEI thickness, and (b) the log ICL. The analysis identified sensitive and insensitive input parameters in both instances.

density, the particle radius of the graphite particles, the equilibrium potential for the SEI growth, the diffusion coefficient for Li-ions in the solid phase, the exchange current density for the (de-)intercalation of Li-ions in the graphite and the minimum cut-off potential. Interestingly, four of the most sensitive input parameters for the SEI thickness was a subset of those for the ICL. This corresponds well with the observation from Fig. 4 that there is a strong correlation between the changes in the SEI thickness and the ICL. Sensitive input parameters such as the radius of the graphite particles, the porosity of the electrode and exchange current density for Li-ions (de-)intercalation into the graphite are related to the Brunauer–Emmett–Teller (BET) specific surface area of the positive electrode, the solvated Li-ions intercalation, and the nature of the surface sites for electrolyte decomposition. Based on previous experimental reports, the BET specific surface area and the solvated Li-ions intercalation contributes strongly to the ICL [45]. The nature of the surface of the graphite also plays a significant role in the extent of the ICL [46].

3.6. Exploration of local sensitivities

Fig. 7 shows local SA of the two most sensitive input parameters identified in the global SA of log SEI thickness in the previous section. The local sensitivity analyses were performed using Eq. (14) with the surrogate GP regression model on the input parameters sampled along their entire range of variation while keeping all other inputs fixed at their nominal values (see Table 2). Additionally, the P2D-SEI model was also evaluated along the range of variation of the input parameters post-hoc and numerical differentiation (central method) was used to estimate the local sensitivities. As can be observed in Fig. 7, the predictions of the surrogate GP regression model and the P2D-SEI model are well aligned and the majority of the P2D-SEI model prediction are within the uncertainty of the surrogate GP regression model predictions. The predictions of the P2D-SEI model appear a little noisy, resulting in noisy estimates of the derivatives, while the GP regression model provides a smooth differentiable function.

The applied current density exhibits a nonlinear relationship with the growth of the SEI and this is highly sensitive at low current densities. In principle, at low current densities, large amount of Li ions are consumed to form the SEI due to the amount of time required to reach a given cut-off potential and the slow kinetics at the surface of the electrode. However, at high current densities, the kinetic reaction is very fast and the time required to reach the cut-off potential is less, thus the growth of the SEI, even-though it is at a fast rate does not change significantly as observed in Fig. 7(a). As expected based on Eq. (1), the equilibrium potential for the SEI formation showed a strong linear relationship with the growth of the SEI with a constant sensitivity along its range of input parameters. However, the sensitivity of the equilibrium potential for SEI formation was constant at lower values of the range of input parameters and increased at values between 0.25 and 0.45. This indicates that, even-though there is a linear increase in the SEI at equilibrium potential for the SEI values below 0.25, the amount of SEI formed is not sensitive to the ICL, hence the other degradation mechanisms such as loss of active materials due to the variation in the volume fraction of the active material is the most sensitive mechanism. Local SA plots for all input parameters on both targets of interest are included in the supplementary material.

Fig. 8 shows the interaction of the sensitive inputs along their entire range of variation while keeping all other inputs fixed at their nominal values. The sensitivity of the amount of Li ions inserted into the graphite during charging at a wide range of applied current density on the performance of the half-cell was studied by conducting simulation at different end of charge voltage (Fig. 8(a)). In principle the charge and discharge capacity of the cell is expected to decrease with an increase in the end of charge voltage because the capacity of the cell is directly proportional to the amount of available Li ions inserted into the graphite. However, the proportionality also depends on the amount of Li ions consumed to form the SEI layer. As presented in Fig. 8 and Figure S24a, increasing the end of charge voltage resulted in a decrease in both the SEI layer thickness and the ICL, respectively, at low current densities. This indicates that, by decreasing the end off charge voltage, the SOC of the cell increases. This leads to an increase in the amount of Li ions used in the formation of the SEI resulting in an increase in the ICL. However, the SOC of the cell is directly proportional to the discharge capacity, hence in order to simultaneously reduce the internal resistance of the cell due to the increase in the thickness of the SEI layer and achieve a maximum discharge capacity, the end of charge voltage needs to be optimised. Fig. 8(b) presents the ICL as a function of the graphite particle size at various current densities and the corresponding SA. The particle size is inversely proportional to the BET surface area and from previous studies [45,46], an increase in the BET surface area results in an increase in the ICL due to high electrolyte decomposition and excessive Li-ions loss to the formation of the SEI at low current densities. This is inline with the results presented in Fig. 8(b) and Figure S19 where an increase in the particles size resulted in a decrease in the ICL and a linear decrease in the SEI thickness respectively. However, this trend changed as the current density increased, high ICL was observed at high current densities for both the EOCV and the particle size and similar for all the other variable input parameters even though the SEI thickness decreased as expected. This can be attributed to the fact that at high current densities, the main factor causing capacity loss

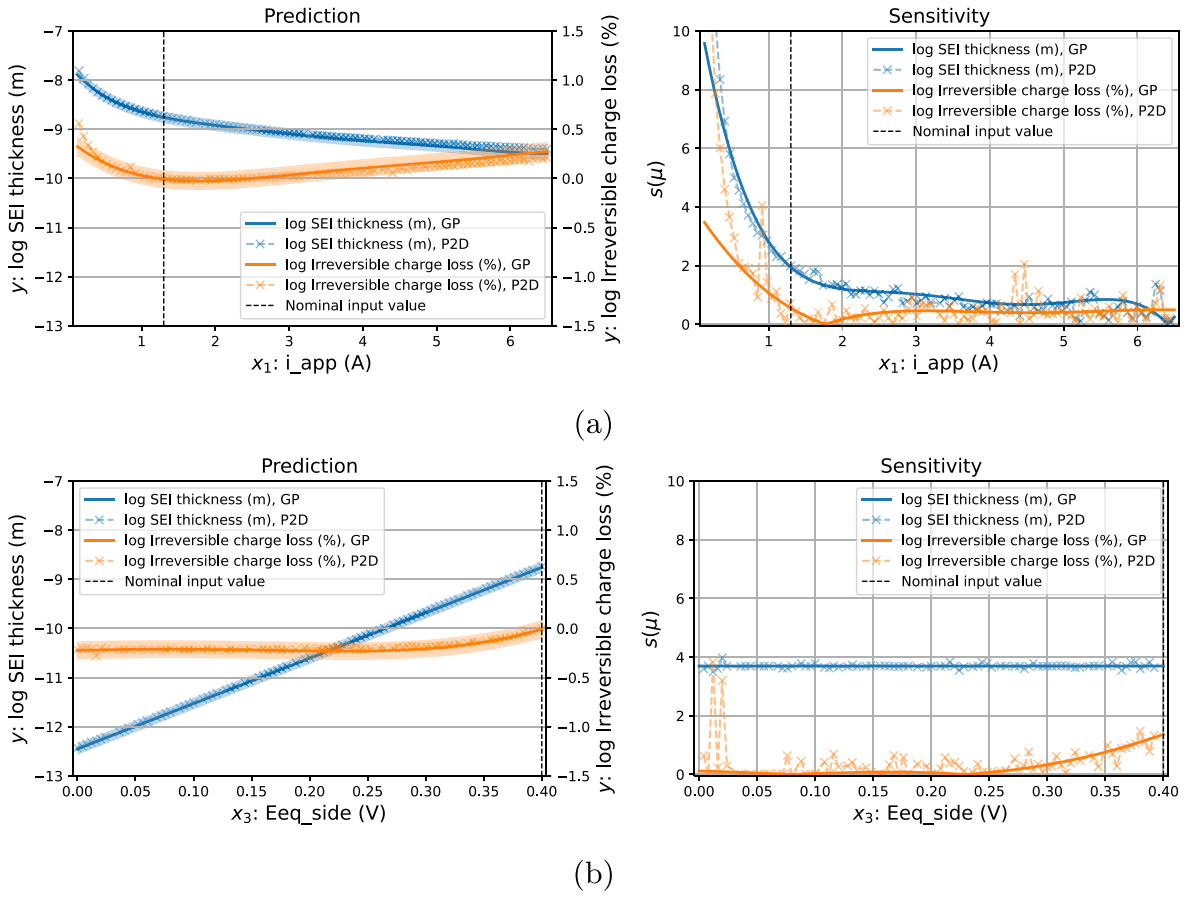

Fig. 7. Local SA of (a) the applied current, and (b) the equilibrium potential of the SEI input parameters along their entire range of variation, while keeping all other inputs fixed at their nominal values, for the log SEI thickness and log ICL outputs, respectively. The solid lines represent predictions made with the Gaussian process surrogate model with the shaded area showing two standard deviations of uncertainty. The dashed lines with crosses represent predictions made with the P2D model. The left plots show the predicted outputs while the right plots show the corresponding local sensitivities. Sensitivities of the GP surrogate model are computed with the derivative method (Eq. (14)) while the sensitivities of the P2D model are estimated with numerical differentiation (central method).

is the overpotential due to the ohmic resistance. In addition to the effect of the changes of EOCV on the ICL and SEI thickness, we also observed an interesting phenomena when other input parameters such as the exchange current density for the (de-)lithiation and SEI formation, and the diffusion coefficient of Li-ions in the graphite. The figures of these fascinating observations are presented in the supplementary material.

3.7. Discussion

In the analysis of local sensitivities in Section 3.6, we presented sensitivity plots of the most sensitive input parameters along their entire range of input values while keeping all other inputs at their nominal values, including sensitivity plots of single input parameters in one dimension (Fig. 7) and interactions of pairs of inputs in two dimensions (Fig. 8). However, the predictions and sensitivities also depend on the values of the remaining inputs because of interactions. For high dimensional inputs it is not feasible to visualise every possible combination of input values, so we have to select only a few interesting input combinations based on domain knowledge or selection criteria defining a specific objective. A major advantage of performing SA with a fast surrogate model is that these plots can be generated fast enough to enable interactive, exploratory SA, where the user can adjust input parameters and immediately see the predicted results visualised. We have created such an interactive application for the global and local SA presented in this work, and made it available online [23]. Screenshots of the interactive application are included in the supplementary material.

Using a surrogate model with uncertainty estimates, such as the GP regression model, provides an opportunity to apply an active learning strategy to generate an informative and diverse training dataset in a sample efficient manner [47]. This is relevant in applications where labelling the samples is expensive or time consuming. We experimented with active learning in our analysis by starting with a small initial training dataset and extending the dataset in an iterative manner by adding batches of diverse examples with high predicted uncertainty. However, we did not observe a significant improvement over random sampling and therefore we left this out of the analysis in the interest of simplicity. We believe this was because in our setup we were able to sample the input space uniformly at random which is already a good strategy for ensuring sample independence and diversity. However, applying active learning might be beneficial in applications where random sampling of the input space is not possible or were generating a large number of samples is not feasible.

In general, the results of a SA with a surrogate model can depend strongly on the range of the input values used to sample the training dataset. Some inputs might have very large effects on the output at extreme values and thus will be assigned high sensitivity locally and on average. If these extreme input values are not considered relevant to the application, they should be removed from the analysis by adjusting the input range accordingly to avoid drawing wrong or misleading conclusions. This kind of large edge effects can be identified through local SA. On the other hand, selecting too narrow input ranges might fail to capture some important effects and lead to wrong or misleading conclusions as well. Note that performing SA on a narrower range of input values can be achieved simply by applying the surrogate model

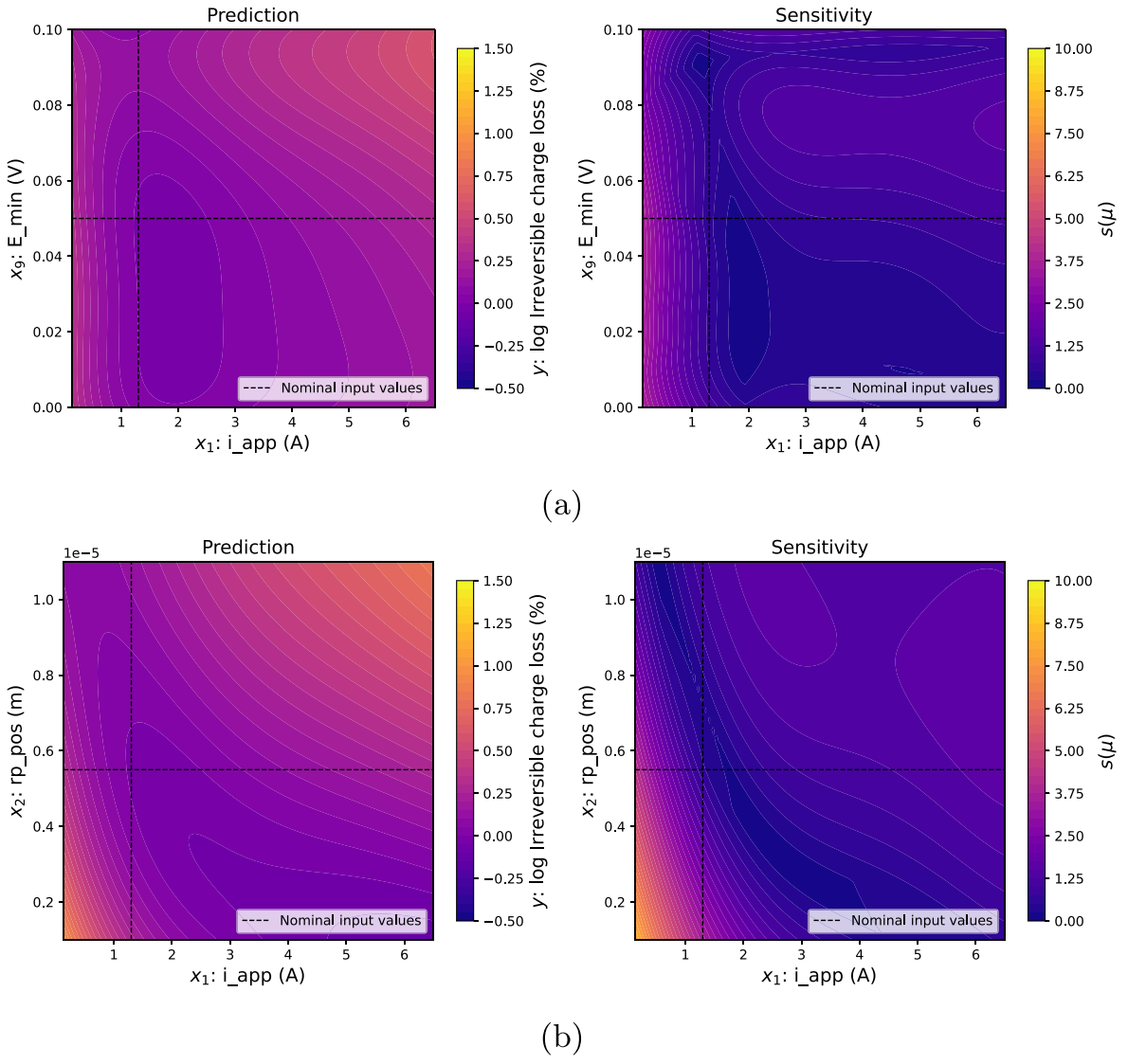

Fig. 8. Local SA for the ICL of relevant sensitive input parameters, (a) applied current and minimum cut-off voltage and (b) applied current and graphite particle radius, along their entire range of variation while keeping all other inputs fixed at their nominal values. The left plots show the predicted log ICL and the right plots shows the corresponding local sensitivity as a function of the inputs.

on a subset of the data, whereas extending the range of input values requires sampling of new data to retrain the surrogate model.

Access to local and global sensitivities of the P2D-SEI model opens up multiple new opportunities in battery research. Knowledge of parameter sensitives allow building of reduced order models based on only the relevant inputs leading to possible light weight battery digital twins. Local sensitives of P2D-SEI model help identify design and operational parameters for long lasting batteries. Most importantly our methodology provides the crucial first step towards building reliable multi-scale battery simulation models with controlled errors propagation from parameter passing between scales. As we obtain clear understanding of correlation between noise in input parameter and errors in output, highly accurate multi-scale simulation frameworks can be built by obtaining important inputs from meticulously done experiments or high quality lower level simulations.

4. Conclusion

In this work, we have presented a continuum scale model that couples the P2D model and a degradation model based on the formation of the SEI (the P2D-SEI model) and demonstrated a detailed global and local SA based on a surrogate GP regression. The analysis centred around two outputs of interest, namely the SEI thickness and the related ICL. The SA identified the globally most sensitive input parameters and provide additional insights about local sensitivities and interactions among these input parameters. The results can be used to identify input parameters that need high-fidelity estimates for the overall model to be accurate. Further exploration of the local sensitivities of the most sensitive input parameters across their entire range of variation revealed linear and nonlinear relationships between the relevant inputs and the outputs, respectively, as well as interactions between the input parameters at different input values. This provided detailed insights into the dynamics of the P2D-SEI model. Based on the SA analysis, it was revealed that, the ICL increases monotonously with an increase in the SEI thickness at low current rates but not at higher current rate. In addition other degradation phenomenon such loss of active materials was discovered during the SA analysis owing the variation in the descriptor parameters in the P2D model. The SA method applied in this paper provides a general and scalable approach to global and local SA that we believe can be applied to a wide range of applications within the battery research community.

CRediT authorship contribution statement

Williams Agyei Appiah: Developed the P2D-SEI model and performed physics-based simulations, Discussion and formal analysis of results, Prepared the first draft. **Jonas Busk:** Developed and implemented the machine learning and SA framework, Discussion and formal analysis of results, Prepared the first draft. **Tejs Vegge:** Discussion and formal analysis of results, Review & editing, Funding acquisition. **Arghya Bhowmik:** Conceptualisation, Supervision, Discussion and formal analysis of results, Review & editing, Funding acquisition.

Declaration of competing interest

The authors declare that they have no known competing financial interests or personal relationships that could have appeared to influence the work reported in this paper.

Data availability

We made the data and code openly accessible in public repository.

Acknowledgements

The authors acknowledge the European Union's Horizon 2020 research and innovation program under grant agreement No 957189 (BIG-MAP) and No 957213 (BATTERY2030PLUS).

Appendix A. Supplementary data

Supplementary material related to this article can be found online at https://doi.org/10.1016/j.electacta.2022.141430.

References

[1] Julia Amici, Pietro Asinari, Elixabete Ayerbe, Philippe Barboux, Pascale Bayle-Guillemaud, R Jürgen Behm, Maitane Berecibar, Erik Berg, Arghya Bhowmik, Silvia Bodoardo, et al., A Roadmap for Transforming Research to Invent the Batteries of the Future Designed within the European Large Scale Research Initiative BATTERY 2030+, Adv. Energy Mater. 2102785.

[2] Arghya Bhowmik, Maitane Berecibar, Montse Casas-Cabanas, Gabor Csanyi, Robert Dominko, Kersti Hermansson, M Rosa Palacin, Helge S Stein, Tejs Vegge, Implications of the BATTERY 2030+ AI-Assisted Toolkit on Future Low-TRL Battery Discoveries and Chemistries, Adv. Energy Mater. 2102698.

[3] Teo Lombardo, Marc Duquesnoy, Hassna El-Bouysidy, Fabian Årén, Alfonso Gallo-Bueno, Peter Bjørn Jørgensen, Arghya Bhowmik, Arnaud Demortière, Elixabete Ayerbe, Francisco Alcaide, et al., Artificial intelligence applied to battery research: hype or reality?, Chem. Rev..

[4] Arghya Bhowmik, Ivano E Castelli, Juan Maria Garcia-Lastra, Peter Bjørn Jørgensen, Ole Winther, Tejs Vegge, A perspective on inverse design of battery interphases using multi-scale modelling, experiments and generative deep learning, Energy Storage Mater. 21 (2019) 446–456.

[5] Maximilian Fichtner, Kristina Edström, Elixabete Ayerbe, Maitane Berecibar, Arghya Bhowmik, Ivano E Castelli, Simon Clark, Robert Dominko, Merve Erakca, Alejandro A Franco, et al., Rechargeable Batteries of the Future—The State of the Art from a BATTERY 2030+ Perspective, Adv. Energy Mater. 2102904.

[6] Diddo Diddens, Williams Agyei Appiah, Youssef Mabrouk, Andreas Heuer, Tejs Vegge, Arghya Bhowmik, Modeling the solid electrolyte interphase: Machine learning as a game changer? Adv. Mater. Interfaces 9 (8) (2022) 2101734.

[7] Alejandro A Franco, Alexis Rucci, Daniel Brandell, Christine Frayret, Miran Gaberscek, Piotr Jankowski, Patrik Johansson, Boosting rechargeable batteries R&D by multiscale modeling: myth or reality? Chem. Rev. 119 (7) (2019) 4569–4627.

[8] Bertrand Iooss, Paul Lemaître, A Review on Global Sensitivity Analysis Methods, Springer US, Boston, MA, 2015, pp. 101–122.

[9] Alexander P Schmidt, Matthias Bitzer, Árpád W Imre, Lino Guzzella, Experiment-driven electrochemical modeling and systematic parameterization for a lithium-ion battery cell, J. Power Sources 195 (15) (2010) 5071–5080.

[10] Habiballah Rahimi-Eichi, Bharat Balagopal, Mo-Yuen Chow, Tae-Jung Yeo, Sensitivity analysis of lithium-ion battery model to battery parameters, in: IECON 2013-39th Annual Conference of the IEEE Industrial Electronics Society, IEEE, 2013, pp. 6794–6799.

[11] Liqiang Zhang, Chao Lyu, Gareth Hinds, Lixin Wang, Weilin Luo, Jun Zheng, Kehua Ma, Parameter sensitivity analysis of cylindrical LiFePO4 battery performance using multi-physics modeling, J. Electrochem. Soc. 161 (5) (2014) A762.

[12] Minseok Song, Song-Yul Choe, Parameter sensitivity analysis of a reduced-order electrochemical-thermal model for heat generation rate of lithium-ion batteries, Appl. Energy 305 (2022) 117920.

[13] Shi Zhao, David A. Howey, Global sensitivity analysis of battery equivalent circuit model parameters, in: 2016 IEEE Vehicle Power and Propulsion Conference (VPPC), IEEE, 2016, pp. 1–4.

[14] Max D. Morris, Factorial sampling plans for preliminary computational experiments, Technometrics 33 (2) (1991) 161–174.

[15] Nan Lin, Xiangzhong Xie, René Schenkendorf, Ulrike Krewer, Efficient global sensitivity analysis of 3D multiphysics model for Li-ion batteries, J. Electrochem. Soc. 165 (7) (2018) A1169.

[16] Géraud Blatman, Bruno Sudret, An adaptive algorithm to build up sparse polynomial chaos expansions for stochastic finite element analysis, Probab. Eng. Mech. 25 (2) (2010) 183–197.

[17] Christopher K. Williams, Carl Edward Rasmussen, Gaussian Processes for Machine Learning, Vol. 2, (3) MIT press Cambridge, MA, 2006.

[18] Joaquin Quiñonero-Candela, Carl Edward Rasmussen, A unifying view of sparse approximate Gaussian process regression, J. Mach. Learn. Res. 6 (65) (2005) 1939–1959.

[19] Michalis Titsias, Variational learning of inducing variables in sparse Gaussian processes, in: David van Dyk, Max Welling (Eds.), Proceedings of the Twelth International Conference on Artificial Intelligence and Statistics, Vol. 5, in: Proceedings of Machine Learning Research, PMLR, Hilton Clearwater Beach Resort, Clearwater Beach, Florida USA, 2009, pp. 567–574.

[20] Topi Paananen, Juho Piironen, Michael Riis Andersen, Aki Vehtari, Variable selection for Gaussian processes via sensitivity analysis of the posterior predictive distribution, in: The 22nd International Conference on Artificial Intelligence and Statistics, PMLR, 2019, pp. 1743–1752.

[21] Peter Mondrup Rasmussen, Kristoffer Hougaard Madsen, Torben Ellegaard Lund, Lars Kai Hansen, Visualization of nonlinear kernel models in neuroimaging by sensitivity maps, NeuroImage 55 (3) (2011) 1120–1131.

[22] Katalin Blix, Gustau Camps-Valls, Robert Jenssen, Gaussian process sensitivity analysis for oceanic chlorophyll estimation, IEEE J. Sel. Top. Appl. Earth Obs. Remote Sens. 10 (4) (2017) 1265–1277.

[23] Interactive sensitivity analysis software: https://github.com/big-map/sa_p2d_sei_interactive.

[24] Satu Kristiina Heiskanen, Jongjung Kim, Brett L. Lucht, Generation and evolution of the solid electrolyte interphase of lithium-ion batteries, Joule 3 (10) (2019) 2322–2333.

[25] Marc Doyle, Thomas F. Fuller, John Newman, Modeling of galvanostatic charge and discharge of the lithium/polymer/insertion cell, J. Electrochem. Soc. 140 (6) (1993) 1526.

[26] Thomas F. Fuller, Marc Doyle, John Newman, Simulation and optimization of the dual lithium ion insertion cell, J. Electrochem. Soc. 141 (1) (1994) 1.

[27] Atilim Gunes Baydin, Barak A Pearlmutter, Alexey Andreyevich Radul, Jeffrey Mark Siskind, Automatic differentiation in machine learning: a survey, J. Marchine Learn. Res. 18 (2018) 1–43.

[28] Joongpyo Shim, Kathryn A. Striebel, Effect of electrode density on cycle performance and irreversible capacity loss for natural graphite anode in lithium-ion batteries, J. Power Sources 119 (2003) 934–937.

[29] Seon-Hong Lee, Ho-Gon You, Kyu-Suk Han, Jake Kim, In-Ho Jung, Joo-Han Song, A new approach to surface properties of solid electrolyte interphase on a graphite negative electrode, J. Power Sources 247 (2014) 307–313.

[30] Seong Jin An, Jianlin Li, Claus Daniel, Debasish Mohanty, Shrikant Nagpure, David L Wood III, The state of understanding of the lithium-ion-battery graphite solid electrolyte interphase (SEI) and its relationship to formation cycling, Carbon 105 (2016) 52–76.

[31] Yverick Rangom, Timothy T. Duignan, X.S. Zhao, Lithium-ion transport behavior in thin-film graphite electrodes with SEI layers formed at different current densities, ACS Appl. Mater. Interfaces 13 (36) (2021) 42662–42669.

[32] Williams Agyei Appiah, Joonam Park, Seoungwoo Byun, Myung-Hyun Ryou, Yong Min Lee, A mathematical model for cyclic aging of spinel LiMn2O4/graphite lithium-ion cells, J. Electrochem. Soc. 163 (13) (2016) A2757.

[33] Jonas Keil, Andreas Jossen, Electrochemical modeling of linear and nonlinear aging of lithium-ion cells, J. Electrochem. Soc. 167 (11) (2020) 110535.

[34] Shi-chun Yang, Yang Hua, Dan Qiao, Yu-bo Lian, Yu-wei Pan, Yong-ling He, A coupled electrochemical-thermal-mechanical degradation modelling approach for lifetime assessment of lithium-ion batteries, Electrochim. Acta 326 (2019) 134928.

[35] Andrea Lamorgese, Roberto Mauri, Bernardo Tellini, Electrochemical-thermal P2D aging model of a LiCoO2/graphite cell: Capacity fade simulations, J. Energy Storage 20 (2018) 289–297.

[36] Mengyun Nie, Dinesh Chalasani, Daniel P Abraham, Yanjing Chen, Arijit Bose, Brett L Lucht, Lithium ion battery graphite solid electrolyte interphase revealed by microscopy and spectroscopy, J. Phys. Chem. C 117 (3) (2013) 1257–1267.

[37] P Ramadass, Bala Haran, Parthasarathy M Gomadam, Ralph White, Branko N Popov, Development of first principles capacity fade model for Li-ion cells, J. Electrochem. Soc. 151 (2) (2004) A196.
[38] Yuki Yamada, Jianhui Wang, Seongjae Ko, Eriko Watanabe, Atsuo Yamada, Advances and issues in developing salt-concentrated battery electrolytes, Nat. Energy 4 (4) (2019) 269–280.
[39] Weihan Li, Decheng Cao, Dominik Jöst, Florian Ringbeck, Matthias Kuipers, Fabian Frie, Dirk Uwe Sauer, Parameter sensitivity analysis of electrochemical model-based battery management systems for lithium-ion batteries, Appl. Energy 269 (2020) 115104.
[40] Williams Agyei Appiah, Myung-Hyun Ryou, Yong Min Lee, A physics-based model capacity fade analysis of LiMn2O4/graphite cell at different temperatures, J. Electrochem. Soc. 166 (3) (2018) A5109.
[41] Kristen A Severson, Peter M Attia, Norman Jin, Nicholas Perkins, Benben Jiang, Zi Yang, Michael H Chen, Muratahan Aykol, Patrick K Herring, Dimitrios Fraggedakis, et al., Data-driven prediction of battery cycle life before capacity degradation, Nat. Energy 4 (5) (2019) 383–391.
[42] Williams Agyei Appiah, Joonam Park, Seoungwoo Byun, Youngjoon Roh, Myung-Hyun Ryou, Yong Min Lee, Time-effective accelerated cyclic aging analysis of lithium-ion batteries, ChemElectroChem 6 (14) (2019) 3714–3725.
[43] Eli Bingham, Jonathan P. Chen, Martin Jankowiak, Fritz Obermeyer, Neeraj Pradhan, Theofanis Karaletsos, Rohit Singh, Paul Szerlip, Paul Horsfall, Noah D. Goodman, Pyro: Deep Universal Probabilistic Programming, J. Mach. Learn. Res. (2018).
[44] Pankaj Arora, Ralph E. White, Marc Doyle, Capacity fade mechanisms and side reactions in lithium-ion batteries, J. Electrochem. Soc. 145 (10) (1998) 3647.
[45] Martin Winter, Petr Novák, Alain Monnier, Graphites for lithium-ion cells: the correlation of the first-cycle charge loss with the brunauer-emmett-teller surface area, J. Electrochem. Soc. 145 (2) (1998) 428.
[46] Karim Zaghib, Gabrielle Nadeau, Kimio Kinoshita, Effect of graphite particle size on irreversible capacity loss, J. Electrochem. Soc. 147 (6) (2000) 2110.
[47] Burr Settles, Active learning literature survey, 2009.